Fabrication of $CuInTe_2$ and $CuInTe_{2-x}Se_x$ Ternary Gradient Quantum Dots and Their Application to Solar Cells

Sungwoo Kim,[†,∥] Meejae Kang,[†,∥] Seajin Kim,[†] Jin-Hyuk Heo,[§] Jun Hong Noh,[‡] Sang Hyuk Im,[§,*] Sang Il Seok,[‡,⊥,*] and Sang-Wook Kim[†,*]

[†]Department of Molecular Science and Technology, Ajou University, Suwon 443-749, Republic of Korea, [‡]Solar Energy Materials Research Group, Advanced Materials Division, Korea Research Institute of Chemical Technology, 141 Gajeong-ro, Yuseong-gu, Daejeon 305-600, Republic of Korea, [§]Department of Chemical Engineering, College of Engineering, Kyung Hee University, 1 Seochon-dong, Giheung-gu, Youngin-si, Gyeonggi-do 446-701, Republic of Korea, and [⊥]Department of Energy Science, Sungkyunkwan University, Suwon 440-746, Republic of Korea. [∥]These two authors contributed equally to this work.

ABSTRACT We report the first synthesis of colloidal $CuInTe_2$, $CuInTe_{2-x}Se_x$ gradient alloyed quantum dots (QDs) through a simple hot injection method. We confirmed the composition of synthesized QDs to cationic rich phase of $CuIn_{1.5}Te_{2.5}$ and $Cu_{0.23}In_{0.36}Te_{0.19}Se_{0.22}$ with XPS and ICP analysis, and we have also found that the gradient alloyed $Cu_{0.23}In_{0.36}Te_{0.19}Se_{0.22}$ QDs exhibit greatly improved stability over the $CuIn_{1.5}Te_{2.5}$ QDs. The solution-processed solar cell based on the gradient alloyed $Cu_{0.23}In_{0.36}Te_{0.19}Se_{0.22}$ QDs exhibited 17.4 mA/cm^2 of short circuit current density (J_{sc}), 0.40 V of open circuit voltage (V_{oc}), 44.1% of fill factor (FF), and 3.1% of overall power conversion efficiency at 100 mW/cm^2 AM 1.5G illumination.

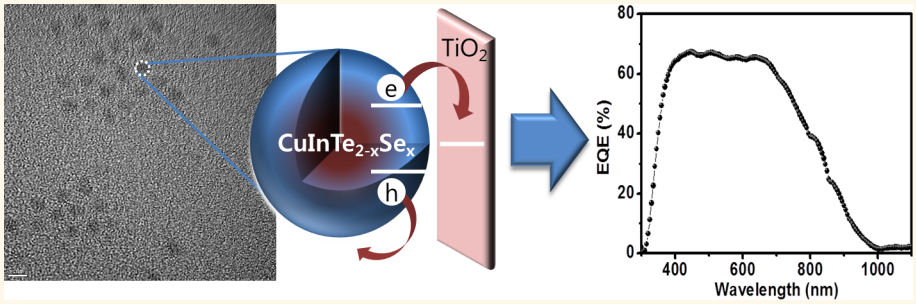

KEYWORDS: quantum dots · $CuInTe_2$ · $CuInTe_{2-x}Se_x$ · gradient alloyed quantum dot · solar cell

Colloidal quantum dots (QDs) have received considerable attention owing to their size-tunable properties and their application to light-emitting diodes (LEDs),[1−4] solar cells,[5−9] biolabeling,[10−12] and so on. In particular, I−III−VI QDs such as $CuInS_2$[13−20] and $CuInSe_2$[21−28] have been considered as candidates for solar cells, and consequently, extensive research has been conducted to understand their synthesis and application. $CuInTe_2$ is also a I−III−VI semiconductor with a direct band gap of 1.02 eV in the bulk state, which is smaller than that in the cases of $CuInS_2$ and $CuInSe_2$. $CuInTe_2$ exhibits a stronger quantum confinement effect and a larger Bohr radius than $CuInS_2$ and $CuInSe_2$, owing to the covalent property of tellurium.[53] $CuInTe_2$ films have been widely used for photovoltaic devices as they have a high energy conversion efficiency.[38] The $CuInTe_2$ film can be fabricated through microwave irradiation, polyol synthesis, a silicate matrix method, and so on.[32−40] However, few studies have been conducted on colloidal $CuInTe_2$.[39,40] Also, the stability is low due to easily oxidative property of Te, and photophysical properties are not satisfactory. Although the core−shell structure can reduce the lattice stress by the epitaxial growth on the core surface, there is still much stress in the core−shell boundary, which possibly triggers the interfacial defect. In order to further lessen the stress and exploit the effective optical properties, compositional gradient-type QDs were suggested. The CdSe/CdS/$Zn_{0.5}Cd_{0.5}S$/ZnS core/shell gradient QDs were first developed in 2005 by Xie *et al.*[29] Bailey *et al.* reported $CdSe_{1-x}Te_x$ alloy QDs with a Se-rich core and Te-rich shell.[30] Lim *et al.* developed InP/ZnSeS QDs with a gradient shell using the reactivity difference between TOP-S and TOP-Se precursors.[31] In this work, both

* Address correspondence to swkim@ajou.ac.kr, seoksi@krict.re.kr, imromy@khu.ac.kr.

Received for review September 20, 2012 and accepted May 8, 2013.

Published online May 08, 2013
10.1021/nn401274e

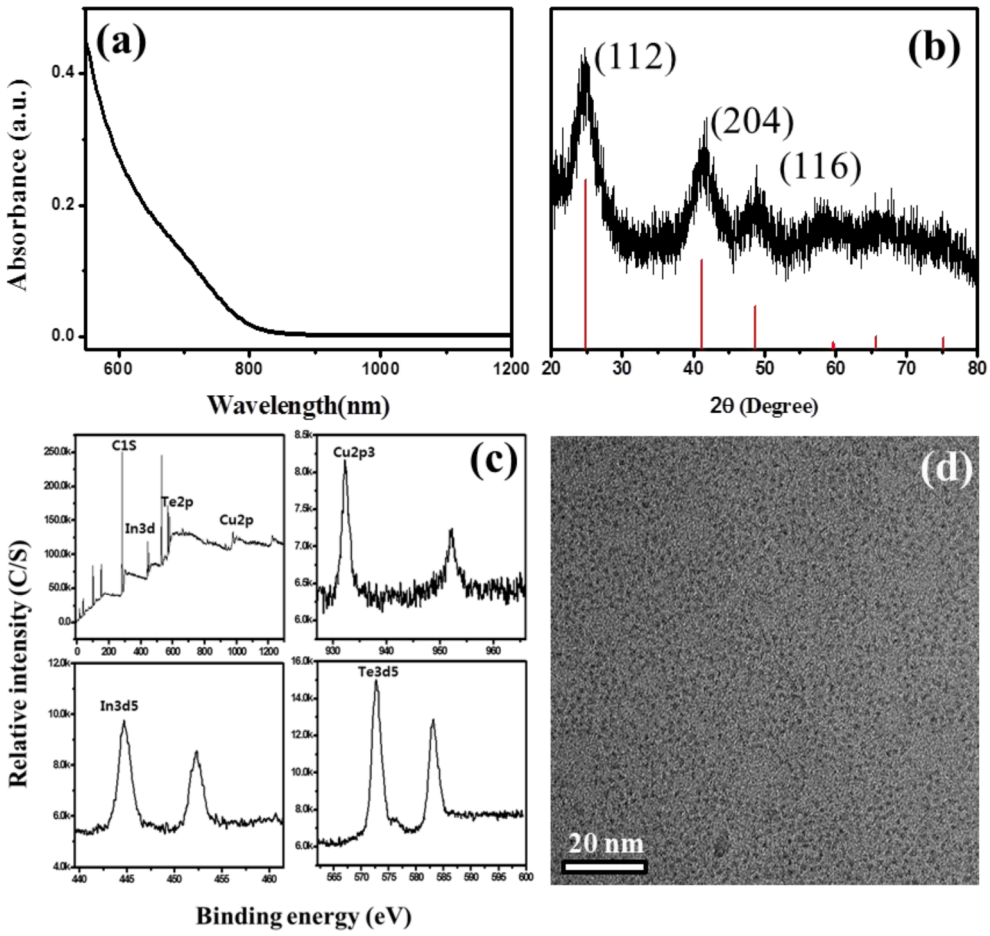

Figure 1. (a) Absorption spectra of $CuInTe_2$ QDs and (b) XRD pattern which indicates (112), (204), and (116) planes of the chalcopyrite structure. (c) XPS spectra of as-synthesized $CuInTe_2$ QDs. (d) TEM images of 2.4−2.8 nm diameter QDs.

new gradient $CuInTe_{2-x}Se_x$ alloy QDs and ternary $CuInTe_2$ QDs have been reported, and their application to solar cells has been proposed.

RESULTS AND DISCUSSION

$CuInTe_2$ ternary QDs were synthesized with copper iodide (CuI), indium acetate ($In(OAc)_3$), and a tri-*n*-octylphosphine telluride (TOP-Te) stock solution as precursors and 1-dodecanethiol (DDT) as a surfactant. The TOP-Te solution was added to a degassed 1-octadecene (ODE) solution at room temperature, and the solution was heated to 250 °C. Then, a Cu−In complex solution was rapidly injected to the solution under N_2 atmosphere, and the mixture was immediately cooled to room temperature. The detailed experimental procedure is provided in the Experimental Section. The resultant $CuInTe_2$ ternary QDs showed an excitonic absorption peak at approximately 720 nm (Figure 1a). However, very weak photoluminescence (PL) was observed owing to the trap site by lattice defects. Figure 1b shows the powder X-ray diffraction (PXRD) patterns of $CuInTe_2$ QDs, which show three prominent peaks. These peaks are indexed to the (112), (204), and (116) planes of the chalcopyrite structure of the $CuInTe_2$ QDs, which is in good agreement with the data of the bulk $CuInTe_2$ (#JCPDS 82-0450). Figure 1c shows the X-ray photoelectron spectroscopy (XPS) data of $CuInTe_2$ QDs. The survey spectrum indicates the existence of Cu, In, and Te, as well. The Cu2p3, In3p5, and Te3d5 binding energy peaks were observed at 932.7, 444.8, and 572.8 eV, respectively, which confirms the existence of Cu^+, In^{3+}, and Te^{2-}.[41] In the Te spectrum, a broad and small tellurium oxide peak was observed at 576 eV, indicating the easily oxidative property of Te. The elemental composition was measured by inductively coupled plasma atomic emission spectroscopy (ICP-AES). According to the results, the molar ratios of Cu/In/Te are about 1:1.5:2.5, which indicates that the quantity of In and Te is richer than that of Cu, in contrast to the stoichiometric ratio (1:1:2). The cationic property because of Cu^+ and In^{3+} ions is predominant over the Te^{2-} anion. These data imply that anionic sites in the tetrahedral hole are more likely to have lattice defects than the cationic site of the structure framework. The quantitative tendency could be also verified from the integrated areas of the Cu2p3, In3p5, and Te3d5 peaks in the XPS spectrum. Figure 1d is the transmission electron microscopy (TEM) image of $CuInTe_2$ ternary QDs, which shows the nanocrystals of

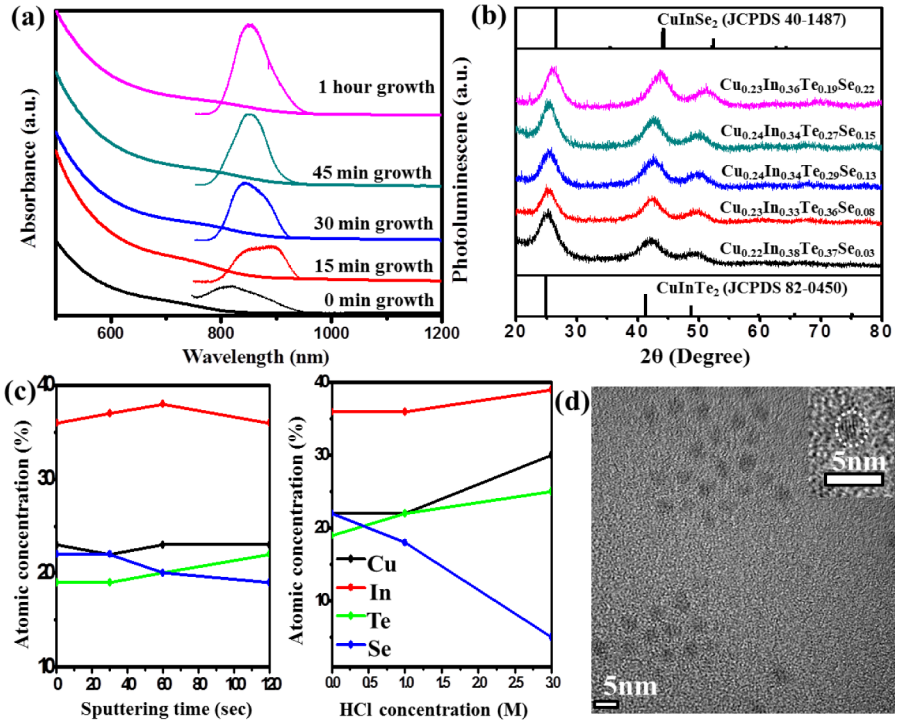

Figure 2. Compositional change of (a) absorption and emission spectra and (b) XRD patterns. (c) Atomic content of $Cu_{0.23}In_{0.36}Te_{0.19}Se_{0.22}$ alloyed QDs with ion sputtering and HCl etching. (d) TEM image of the sample at 1 h and the magnified image.

approximately 2.4 nm diameter after size selection. The mean particle diameter can also be determined from the Debye−Scherrer equation, which uses the full width at half-maximum (fwhm) of the diffraction peaks. We chose the (112) plane and calculated the equation, which showed a similar result, a 2.8 nm diameter. The fabrication of colloidal $CuInTe_2$ QDs was done successfully; however, their optical and application properties were not noticeable. We designed new alloyed $CuInTe_{2-x}Se_x$ QDs to improve the photophysical properties of $CuInTe_2$ QDs. The better stability of selenium compared with tellurium results in advancement of properties, which can endow the potential for various applications.

For the representative synthesis of $CuInTe_{2-x}Se_x$ alloy QDs, a prepared thiol complex solution, which included Cu, In, and Te precursors, was injected to a degassed ODE solution already containing TOP-Se at 250 °C under N_2 atmosphere. The precursor ratio of Cu/In/Te/Se was 1:1:1:2. After the injection, the solution was cooled to 200 °C and maintained for 1 h. Then, the solution was purified through precipitation in an excess of ethanol and through subsequent centrifugation. The detailed experimental procedure is provided in the Experimental Section.

To study the physical properties and stoichiometry of the growing alloyed dots, aliquots of the reaction solution were sampled at 0, 15, 30, 45, and 60 min. The chemical compositions of QDs were determined through ICP-AES. Elemental analysis showed that each sample has a similar ratio of Cu and In and an increased Se/Te ratio during the growth. The particle size also increased with the growth (Supporting Information Figure S1). From the data, we can speculate that the $CuInTe_{2-x}Se_x$ QDs are gradient alloys with the highest selenium content at the surface. The Cu/In/Te/Se precursor ratio of 1:1:1:2 resulted in $Cu_{0.23}In_{0.36}Te_{0.19}Se_{0.22}$ alloy QDs. The composition implies that the dots are still indium-rich and have a cation-predominant structure and that the Te precursors are more reactive as compared with Se precursors. We performed the same reaction with different precursor ratios; for example, for a higher Te composition (Te/Se = 1/1), aggregation of QDs occurred. Figure 2a shows the temporal evolution of the emission and absorption spectra of the $CuInTe_{2-x}Se_x$ alloy QDs. After the Cu−In−Te complex solution was injected, the first excitonic absorption peak appeared approximately at 700 nm (Figure 2a, black solid line). As the growth occurred gradually, the absorption peak finally shifted to 800 nm (Figure 2a, pink solid line). Photoluminescence showed a trap site and band emission until 30 min of growth time at the same time (Figure 2a, blue solid line). After 1 h, the alloy QDs showed emission peaks at approximately 855 nm (Figure 2a, pink solid line). The data indicate that the trap site can be effectively suppressed by selenium near the surface, thus inhibiting the generation of vacancies.

To understand the better stability of selenium compared with tellurium, we compared XPS data, as shown in Figure S3. From the 576 eV of tellurium oxide at high-resolution XPS peak analyses, we can see that the $CuInTe_2$ QDs were oxidized to TeO_2 while the $CuInTe_{2-x}Se_x$ alloy QDs did not show an oxide peak. Here, it should be noted that $CuInTe_{2-x}Se_x$ alloy QDs provided good air stability. PXRD also demonstrated the structure of the gradient

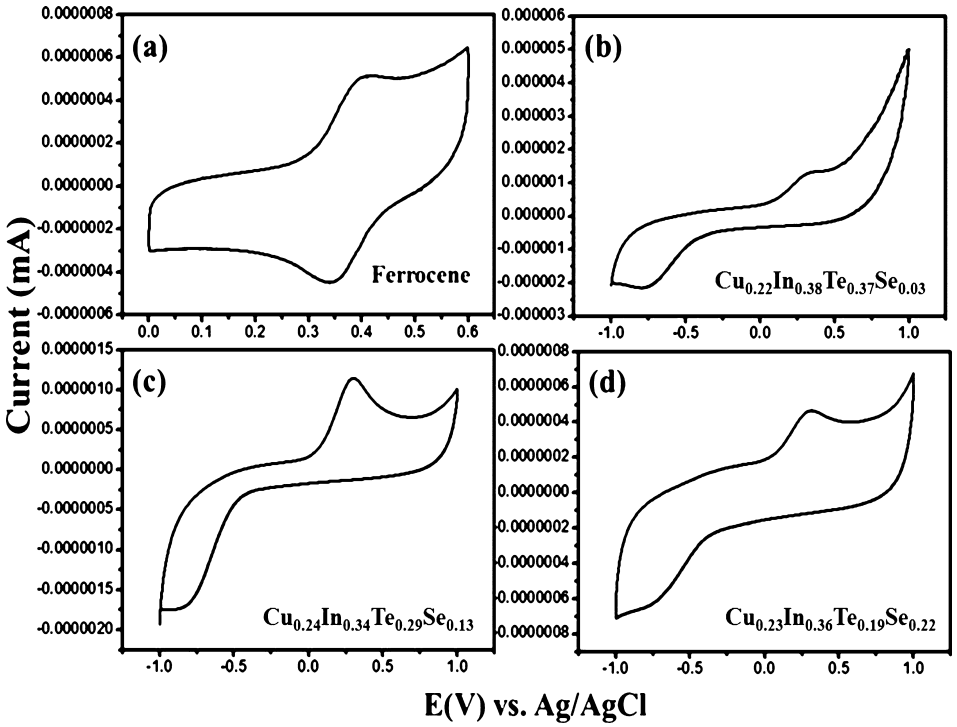

Figure 3. Cyclic votammogram of $CuInTe_{2-x}Se_x$ nanoparticles at different reaction times and ferrocene.

$CuInTe_{2-x}Se_x$ alloy QDs. Figure 2b shows the compositional change in the PXRD pattern of the $CuInTe_{2-x}Se_x$ alloy QDs. As the growth occurred, the diffraction peaks gradually shifted toward bulk $CuInSe_2$. This implies high content of Se in the outside region, considering the increase in particle size with time (Figure S4). To clarify the gradient internal structure, we attempted ion sputtering and etching experiment using HCl (Figure 2c). Though both data are not quantitatively accurate, they show decreased selenium and increased tellurium content, indicating richer selenium close to the surface of the dots. TEM and magnified TEM images of $Cu_{0.23}In_{0.36}Te_{0.19}Se_{0.22}$ alloy QDs show nearly monodispersed 4 nm dots with crystallinity (Figure 2d). Figure S1 shows that the particle sizes increase from 2.5 to 4.0 nm with a standard deviation of 10−15% as the Se mole fraction changes from 0.09 to 0.23.

In addition, we could observe all components including Cu, In, Te, and Se in the STEM-EDX data (Figure S2). To apply the QDs to solar cells, band offsets should be determined. Cyclic voltammetry (CV) measurement is an easy and effective approach to evaluate the position of both the highest occupied molecular orbital (HOMO) and the lowest unoccupied molecular orbital (LUMO) energy levels.[42−52] Figure 3 shows the CV data of $CuInTe_{2-x}Se_x$ QDs at different reaction time and ferrocene as a reference. The HOMO (or LUMO) levels of QDs are calculated from the onset of the oxidation peak and HOMO (or LUMO) of ferrocene using the following equation.

$$\text{HOMO (orLUMO) (eV)} = -4.8 - [(E_{\text{onset}} - E1/2(\text{ferrocene})]$$

The value of −4.8 eV was obtained by the vacuum energy level of ferrocene with Ag/AgCl reference electrode. Figure 2d shows the CV data of the $Cu_{0.23}In_{0.36}Te_{0.19}Se_{0.22}$ QDs. The CV data exhibited the onset of an oxidation peak at 0.1 V and the onset of a reduction peak at −4.7 V with the Ag/AgCl reference electrode. The HOMO and LUMO levels of the sample are −4.6 and −3.2 eV, respectively, for a band gap of 1.40 eV.

To apply the synthesized $Cu_{0.23}In_{0.36}Te_{0.19}Se_{0.22}$ (CITSe) QDs to solar cells, we simply fabricated an n−p heterojunction solar cell, as depicted in Figure 4a. We constructed the solar cell with FTO/bl-TiO_2/mp-TiO_2/CITSe QDs/Au as the transparent conducting electrode/blocking layer/n-type wide band gap semiconductor/p-type narrow band gap semiconductor/counter electrode layer. For the formation of multiply layered CITSe QDs, we spin-coated the CITSe QD solution on the 3-mercaptopropionic acid (3-MPA)-treated FTO/bl-TiO_2/mp-TiO_2 film and repeatedly spin-coated 1 wt % of 1,2-ethanedithiol (EDT)/ethanol solution and CITSe QD solution. Here, the 3-MPA on the surface of mp-TiO_2 helps the CITSe QDs to be uniformly coated on the surface of TiO_2 and the EDT molecules more closely link the CITSe QDs. Upon illumination from external light, the CITSe QDs absorb the light and generate electron−hole pairs, as shown in Figure 4b. The generated electrons are then transported to the TiO_2 electrode, and simultaneously, the holes travel to the multiply packed CITSe QD layer before reaching the Au electrode. The SEM cross-sectional image of the real device in Figure 4c shows that, apparently, the CITSe QDs are well infiltrated in the pore of a 1 μm thick mp-TiO_2 film and form a ~50 nm thick overlayer on top of mp-TiO_2 film because we used relatively larger single-crystalline TiO_2 nanoparticles (particle size = ~60 nm, anatase).

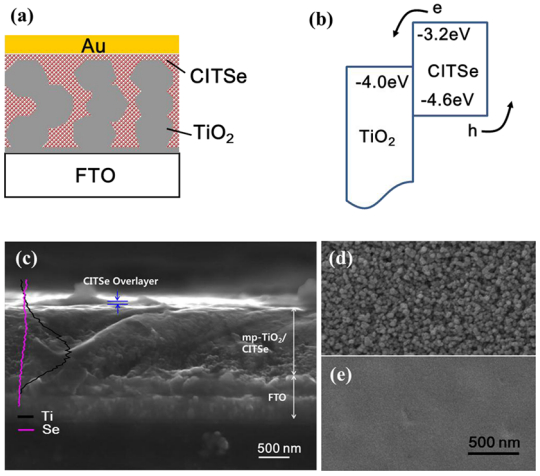

Figure 4. (a) Schematic illustration of device architecture, (b) energy band diagram, (c) SEM cross-sectional image of real device; the inset exhibits the EDS line profile of Ti and Se. SEM top-surface images of (d) bare mp-TiO_2 film and (e) CITSe QDs deposited on mp-TiO_2 film.

The EDS line profiles of Ti and Se in the SEM cross-sectional image confirm that the CITSe QDs are infiltrated into the bottom of the mp-TiO_2 layer. Figure 3d,e shows the SEM surface images of the bare TiO_2 film without a CITSe QD layer and TiO_2 film coated with a CITSe QD layer. These images clearly indicate that the top surface of mp-TiO_2 film was fully covered by a CITSe QD overlayer.

Figure 5 exhibits the device performance of CITSe QD-based heterojunction solar cells with and without heat treatment because it is well-known that either a postchemical treatment in EDT solution or a heat treatment can improve the device efficiency owing to the improved interfacial contact between colloidal quantum dots. Hence we compared the pristine (CITSe-pristine) and the post-heat-treated (CITSe-heat treated) CITSe QD solar cells. Figure 5a shows that both devices exploit the light up to the 1000 nm wavelength region, and the post-heat-treated one has more improved external quantum efficiency (EQE), displaying over 60% across the entire visible region. The more broadened EQE spectrum, up to a 1000 nm wavelength, than the band gap of the CITSe colloidal QDs (E_g = 1.45 eV) might be associated with the interaction of tightly packed QDs by short EDT linker molecules. These results confirm that the post heat treatment at 150 °C for 10 min under N_2 atmosphere is effective to improve the performance of a multiply layered CITSe QD-based heterojunction solar cell. Here, it should be noted that the current CITSe QD-based device was fabricated by a simple spin-coating process without

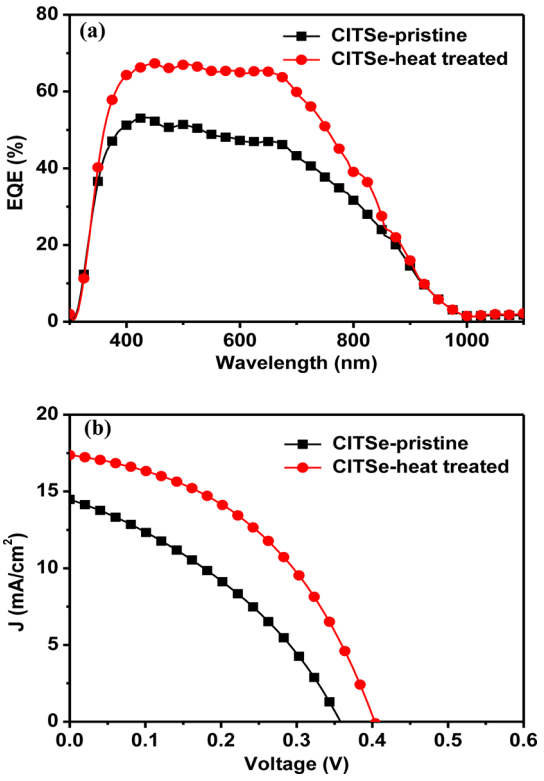

Figure 5. (a) EQE spectra and (b) *J*–*V* curves of pristine (CITSe-pristine) and post-heat-treated (CITSe-heat treated) CITSe QD-based solar cells.

selenization at high temperature or by a toxic hydrazine method. The photocurrent density–voltage (*J*–*V*) curves in Figure 5b indicate that the post-heat-treated CITSe QD device has better efficiency by the improvement of a short circuit current density (J_{sc} = 14.5–17.4 mA/cm^2), an open circuit voltage (V_{oc} = 0.35–0.40 V), a fill factor (FF = 36.2–44.1%), and an overall power conversion efficiency (η = 1.9–3.1%) at 100 mW/cm^2 AM 1.5G illumination.

CONCLUSIONS

In conclusion, we report on the first synthesis of colloidal $CuInTe_2$ and $CuInTe_{2-x}Se_x$ gradient alloyed nanoparticles, achieved through hot injection methods, and we also propose the application of these nanoparticles to solar cells. The band gap of the $Cu_{0.23}In_{0.36}Te_{0.19}Se_{0.22}$ gradient alloyed nanoparticles was determined through CV. The solar cell has a short circuit current density of 17.4 mA/cm^2, an open circuit voltage of 0.40 V, a fill factor of 44.1%, and an overall power conversion efficiency of 3.1% at 100 mW/cm^2 AM 1.5G illumination.

EXPERIMENTAL SECTION

Materials. Copper(I) iodide (99.999%), indium(III) acetate (99.99%), 1-dodecanethiol (98+%), and 1-octadecene (90%) were purchased from Aldrich. Stock solutions of 1 M trioctylphosphine selenide and 1 M trioctylphosphine telluride were prepared by using a selenium pellet (Aldrich, 99.99+%), tellurium powder (Tokyo Chemical Industry, 99.997%), and trioctylphosphine (Strem Chemicals, 97%). Absorption spectra were measured by a

Scinco PDA S-3100 UV/vis spectrophotometer. Transmission electron microscopy (TEM) images and STEM-EDX were taken on a FEI Tecnai G2 F30 Super-Twin transmission electron microscope operating at 300 kV. X-ray diffraction (XRD) patterns were obtained using a Rigaku Ultima III diffractometer equipped with a rotating anode and a Cu Kα radiation source ($\lambda = 0.15418$ nm). Inductively coupled plasma-optical emission spectrometry (ICP-OES) was employed using the OPTIMA 5300DV, PerkinElmer (USA). Cyclic voltammograms of QDs were measured by a CHI624D electrochemical analyzer/workstation.

Preparation of $CuInTe_2$ QDs. Copper iodide (0.2 mmol, 38 mg), indium acetate (0.2 mmol, 58 mg), 2 mL of 1-dodecanethiol, and 1 mL of octadecene were mixed in a 25 mL flask A. The solution was degassed at 90 °C for 2 h. After degassing, the solution cooled to room temperature under nitrogen flow and 0.2 mL of 1 M TOP-Te was added. Octadecene (8 mL) was degassed in another 25 mL flask B at 100 °C for 2 h. Under nitrogen atmosphere, flask B was heated to 250 °C and flask A solution was quickly injected into flask B. After the injection, the solution was cooled to room temperature. Then, the products were precipitated with ethanol and centrifuged to purify the particles.

Preparation of $CuInTe_{2-x}Se_x$ Nanoparticles. Copper iodide (0.2 mmol, 38 mg), indium acetate (0.2 mmol, 58 mg), 2 mL of 1-dodecanethiol, and 1 mL of octadecene were mixed in a 25 mL flask A. The solution was degassed at 90 °C for 2 h. After degassing, the solution cooled to room temperature under nitrogen flow, and 0.4 mL of 0.5 M TOP-Te was added. Octadecene (8 mL) was degassed in another 25 mL flask B at 100 °C for 2 h, and 0.4 mL of 1 M TOP-Se was added. Under nitrogen atmosphere, flask B was heated to 250 °C and flask A solution was quickly injected into flask B. After the injection, the solution was cooled to 200 °C and maintained for 1 h. Then, the products were precipitated with ethanol and centrifuged to purify the particles.

Electrode Preparation for Cyclic Voltammetry. The tests were carried out in a three-electrode system. The used electrodes are glassy carbon electrode as working electrode, platinum wire as counter electrode, and Ag/AgCl electrode as reference electrode. The QDs were dispersed in hexane, and then the samples were added dropwise on the glassy carbon electrode. The measurement was carried out in N_2-saturated acetonitrile solution containing 0.1 M lithium perchlorate ($LiClO_4$), and the scan rate was 50 mV/s.

Argon Ion Etching X-ray Photoelectron Spectroscopy. The data were obtained with a Kα model from Thermo Electron Corporation. The samples were etched using an argon ion gun of 2000 eV for 30 s, 1 min, and 3 min.

Chemical Etching Method with HCl. Two samples of dried QDs (10 mg) were added to a 10 mL vial which contained 2 mL of BuOH. Then, 2 mL of 3 M HCl solution was added to the first sample, and 2 mL of 6 M HCl solution was added to the second sample. Both solutions were mixed by sonication for 2 min. As a result, a two-phase solution consisting of a colored upper phase of butanol and dots and a lower phase of a colorless HCl solution was obtained. The lower phase of HCl solution was removed. The upper phase was reprecipitated with ethanol. Then, ICP measurement was conducted.

Device Fabrication. In a typical procedeure, a 50 nm thick TiO_2 blocking layer (bl-TiO_2) was deposited on a FTO glass (Pilkington, TEC8) by spraying 20 mM titanium diisopropoxide bis(acetylacetonate) solution at 450 °C. A 1 μm thick mp-TiO_2 film (TiO_2 particle size = ~60 nm, anatase phase)[12] was then screen-printed on the bl-TiO_2/FTO substrate and was sintered at 500 °C for 1 h in air atmosphere. The mp-TiO_2 film was dipped in 30 mM of aqueous $TiCl_4$ solution at 60 °C for 1 h, rinsed with pure water, and sintered again at 450 °C for 15 min for the intimate contact between TiO_2 nanoparticles. The $CuInTe_{1-x}Se_x$ solution was then deposited on the mp-TiO_2/bl-TiO_2/FTO substrate by multiple spin-coatings as described in the literature.[13] In a typical deposition process, the mp-TiO_2 film was treated with 10 wt % of 3-mercaptopropionic acid (3-MPA; Aldrich) in ethanolic solution (Burdick & Jackson) to uniformly coat the $CuInTe_{1-x}Se_x$ QDs on the surface of mp-TiO_2. The excess 3-MPA in the mp-TiO_2 film was removed by cleaning with ethanol and chloroform. The 100 μL of $CuInTe_{1-x}Se_x$ QDs in hexane (Aldrich)/1,2-dichlorobenzene (Adrich) (10/1 v/v) solution (15 mg/1 mL) was spin-coated on the 3-MPA-treated mp-TiO_2 film at 2500 rpm for 20 s. In order to form multiply layered $CuInTe_{1-x}Se_x$ QDs, 250 μL of 1 wt % EDT (Aldrich)/ethanol (Burdick & Jackson) solution was spin-coated at 2500 rpm for 20 s, and the $CuInTe_{1-x}Se_x$ QD solution was then spin-coated at 2500 rpm for 20 s. By the repeated spin-coating process of EDT solution and $CuInTe_{1-x}Se_x$ QDs solution, we could form the multiply layered $CuInTe_{1-x}Se_x$ QD films on the mp-TiO_2. Finally, A 60 nm thick Au electrode was then deposited by thermal evaporation under pressure of 5×10^{-5} Torr. For the better electrical contact, a lead pad was formed on the end of FTO and Au electrode by using ultrasonic solder. For the intimate contact between the $CuInTe_{1-x}Se_x$ colloidal quantum dots, the device was then heat-treated at 150 °C for 10 min in N_2 atmosphere. The active area of the device was fixed to 0.16 cm^2.

Device Characterization. The *J*−*V* curves were measured by a source meter (Keithley 2420) and a solar simulator (class A, 91195A; Newport) calibrated by Si reference cell (certified by NREL) at 1 sun and dark state. The *J*−*V* curves were measured by masking the active area with 0.096 cm^2 metal mask. The external quantum efficiency (EQE) spectrum was measured by a light source (300 W Xe lamp, Newport, 66902), a monochromator (Newport Cornerstone 260), and a multimeter (Keithley 2002).

Conflict of Interest: The authors declare no competing financial interest.

Acknowledgment. This work was supported by KRICT 2020 program for Future Technology of the Korea Research Institute of Chemical Technology (KRICT), the Priority Research Centers Program (2012-0006687), and the Industrial Core Technology Development Program funded by the Ministry of Knowledge Economy (No. 10035274), Republic of Korea

Supporting Information Available: Detailed TEM images and I.C.P analysis data at different reaction times of $CuInTe_{2-x}Se_x$ QDs. XPS data and STEM-EDX of $Cu_{0.23}In_{0.36}Te_{0.19}Se_{0.22}$ gradient alloyed QDs. This material is available free of charge *via* the Internet at http://pubs.acs.org.

REFERENCES AND NOTES

1. Coe, S.; Woo, W.-K.; Bawendi, M. G.; Bulovic, V. Electroluminescence from Single Monolayers of Nanocrystals in Molecular Organic Devices. *Nature* **2002**, *420*, 800–803.
2. Zhao, J.; Bardecker, J. A.; Munro, A. M.; Liu, M. S.; Niu, Y.; Ding, I.-K.; Luo, J.; Chen, B.; Jen, A. K.-Y.; Ginger, D. S. Efficient CdSe/CdS Quantum Dot Light-Emitting Diodes Using a Thermally Polymerized Hole Transport Layer. *Nano Lett.* **2006**, *6*, 463–467.
3. Caruge, J. M.; Halpert, J. E.; Wood, V.; Bulovic, V.; Bawendi, M. G. Colloidal Quantum-Dot Light-Emitting Diodes with Metal-Oxide Charge Transport Layers. *Nat. Photonics* **2008**, *2*, 247–250.
4. Kim, S.; Kim, T.; Kang, M.; Kwak, S. K.; Yoo, T. W.; Park, L. S.; Yang, I.; Hwang, S.; Lee, J. E.; Kim, S. K.; *et al.* Highly Luminescent InP/GaP/ZnS Nanocrystals and Their Application to White Light-Emitting Diodes. *J. Am. Chem. Soc.* **2012**, *134*, 3804–3809.
5. Nozik, A. J. Quantum Dot Solar Cells. *Physica E* **2002**, *14*, 115–120.
6. Bang, J. H.; Kamat, P. V. Quantum Dot Sensitized Solar Cells. A Tale of Two Semiconductor Nanocrystals: CdSe and CdTe. *ACS Nano* **2009**, *3*, 1467–1476.
7. Kamat, P. V. Quantum Dot Solar Cells. Semiconductor Nanocrystals as Light Harvesters. *J. Phys. Chem. C* **2008**, *112*, 18737–18735.
8. Kongkanand, A.; Tvrdy, K.; Takechi, K.; Kuno, M.; Kamat, P. V. Quantum Dot Solar Cells. Tuning Photoresponse through Size and Shape Control of CdSe-TiO_2 Architecture. *J. Am. Chem. Soc.* **2008**, *130*, 4007–4015.
9. Pattantyus-Abraham, A. G.; Kramer, I. J.; Barkhouse, A. R.; Wang, X.; Konstantatos, G.; Debnath, R.; Levina, L.; Raabe, I.; Nazeeruddin, M. K.; Grätzel, M.; *et al.* Depleted-Heterojunction Colloidal Quantum Dot Solar Cells. *ACS Nano* **2010**, *4*, 3374–3380.

10. Bharali, D. J.; Lucey, D. W.; Jayakumar, H.; Pudavar, H. E.; Prasad, P. N. Folate-Receptor-Mediated Delivery of InP Quantum Dots for Bioimaging Using Confocal and Two-Photon Microscopy. *J. Am. Chem. Soc.* **2005**, *127*, 11364–11371.
11. Zhang, Y.; Li, Y.; Yan, X.-P. Aqueous Layer-by-Layer Epitaxy of Type-II CdTe/CdSe Quantum Dots with Near-Infrared Fluorescence for Bioimaging Applications. *Small* **2009**, *5*, 185–189.
12. Zaman, M. B.; Baral, T. N.; Zhang, J.; Whitfield, D.; Yu, K. Single-Domain Antibody Functionalized CdSe/ZnS Quantum Dots for Cellular Imaging of Cancer Cells. *J. Phys. Chem. C* **2009**, *113*, 496–499.
13. Nakamura, H.; Kato, W.; Uehara, M.; Nose, K.; Omata, T.; Otsuka-Yao-Matsuo, S.; Miyazaki, M.; Maeda, H. Tunable Photoluminescence Wavelength of Chalcopyrite $CuInS_2$-Based Semiconductor Nanocrystals Synthesized in a Colloidal System. *Chem. Mater.* **2006**, *18*, 3330–3335.
14. Pan, D.; Sun, Z.; Hou, W.; Yang, Y.; Yang, Z.; Lu, Y. Synthesis of Cu-In-S Ternary Nanocrystals with Tunable Structure and Composition. *J. Am. Chem. Soc.* **2008**, *130*, 5620–5621.
15. Xie, R.; Rutherford, M.; Peng, X. Formation of High-Quality I–III–VI Semiconductor Nanocrystals by Tuning Relative Reactivity of Cationic Precursors. *J. Am. Chem. Soc.* **2009**, *131*, 5691–5697.
16. Li, L.; Daou, T. J.; Texier, I.; Chi, T. T. K.; Liem, N. Q.; Reiss, P. Highly Luminescent $CuInS_2$/ZnS Core/Shell Nanocrystals: Cadmium-Free Quantum Dots for *In Vivo* Imaging. *Chem. Mater.* **2009**, *21*, 2422–2429.
17. Batabyal, S. K.; Tian, L.; Venkatram, N.; Ji, W.; Vittal, J. J. Phase-Selective Synthesis of $CuInS_2$ Nanocrystals. *J. Phys. Chem. C* **2009**, *113*, 15037–15042.
18. Li, L.; Pandey, A.; Werder, D. J.; Khanal, B. P.; Pietryga, J. M.; Klimov, V. I. Efficient Synthesis of Highly Luminescent Copper Indium Sulfide-Based Core/Shell Nanocrystals with Surprisingly Long-Lived Emission. *J. Am. Chem. Soc.* **2011**, *133*, 1176–1179.
19. Song, W.-S.; Yang, H. Efficient White-Light-Emitting Diodes Fabricated from Highly Fluorescent Copper Indium Sulfide Core/Shell Quantum Dots. *Chem. Mater.* **2012**, *24*, 1961–1967.
20. Park, J.; Kim, S.-W. $CuInS_2$/ZnS Core/Shell Quantum Dots by Cation Exchange and Their Blue-Shift of Photoluminescence. *J. Mater. Chem.* **2011**, *21*, 3745–3750.
21. Malik, M. A.; O'Brien, P.; Revaprasadu, N. A Novel Route for the Preparation of CuSe and $CuInSe_2$ Nanoparticles. *Adv. Mater.* **1999**, *11*, 1441–1444.
22. Zhang, H.; Li, Y.; Ye, M.; Zhu, Z.; Zhou, Y.; Yang, C.; Li, Y. A Facile Route To Synthesize Chalcopyrite $CuInSe_2$ Nanocrystals in Non-coordinating Solvent. *Nanotechnology* **2007**, *18*, 025602.
23. Allen, P. M.; Bawendi, M. G. Ternary I–III–VI Quantum Dots Luminescent in the Red to Near-Infrared. *J. Am. Chem. Soc.* **2008**, *130*, 9240–9241.
24. Nose, K.; Omata, T.; Otsuka-Yao-Matsuo, S. Colloidal Synthesis of Ternary Copper Indium Diselenide Quantum Dots and Their Optical Properties. *J. Phys. Chem. C* **2009**, *113*, 3455–3460.
25. Cassette, E.; Pons, T.; Bouet, C.; Helle, M.; Bezdetnaya, L.; Marchal, F.; Dubertret, B. Synthesis and Characterization of Near-Infrared Cu-In-Se/ZnS Core/Shell Quantum Dots for *In Vivo* Imaging. *Chem. Mater.* **2010**, *22*, 6117–6124.
26. Wang, J.-J.; Wang, Y.-Q.; Cao, F.-F.; Guo, Y.-G.; Wan, L.-J. Synthesis of Monodispersed Wurtzite Structure $CuInSe_2$ Nanocrystals and Their Application in High-Performance Organic–Inorganic Hybrid Photodetectors. *J. Am. Chem. Soc.* **2010**, *132*, 12218–12221.
27. Zhang, H.; Wang, Z.; Bovero, E.; Lu, Z.; van Veggel, F. C. J. M.; Scholes, G. D. Colloidal $CuInSe_2$ Nanocrystals in the Quantum Confinement Regime: Synthesis, Optical Properties, and Electroluminescence. *J. Phys. Chem. C* **2011**, *115*, 12396–12402.
28. Guo, Q.; Kim, S. J.; Kar, M.; Shafarman, W. N.; Birkmire, R. W.; Stach, E. A.; Agrawal, R.; Hillhouse, H. W. Development of $CuInSe_2$ Nanocrystal and Nanoring Inks for Low-Cost Solar Cells. *Nano Lett.* **2008**, *8*, 2982–2987.
29. Xie, R.; Kolb, U.; Li, J.; Basché, T.; Mews, A. Synthesis and Characterization of Highly Luminescent CdSe-Core CdS/$Zn_{0.5}Cd_{0.5}S$/ZnS Multishell Nanocrystals. *J. Am. Chem. Soc.* **2005**, *127*, 7480–7488.
30. Bailey, E.; Nie, S. Alloyed Semiconductor Quantum Dots: Tuning the Optical Properties without Changing the Particle Size. *J. Am. Chem. Soc.* **2003**, *125*, 7100–7106.
31. Lim, J.; Bae, W. K.; Lee, D.; Nam, M. K.; Jung, J.; Lee, C.; Char, K.; Lee, S. InP@ZnSeS, Core@Composition Gradient Shell Quantum Dots with Enhanced Stability. *Chem. Mater.* **2011**, *23*, 4459–4463.
32. Nadenau, V.; Walter, T.; Schock, H. W. Growth of $CuInTe_2$ Polycrystalline Thin Films. *J. Cryst. Growth* **1995**, *146*, 251–255.
33. Marin, G.; Wasim, S. M.; Perez, G. S.; Bocaranda, P.; Mora, A. E. Compositional, Structural, Optical and Electrical Characterization of $CuInTe_2$ Grown by the Tellurization of Stoichiometric Cu and In in the Liquid Phase. *J. Electron. Mater.* **1998**, *27*, 1351–1357.
34. Ishizaki, T.; Saito, N.; Fuwa, A. Electrodeposition of $CuInTe_2$ Film from an Acidic Solution. *Surf. Coat. Technol.* **2004**, *182*, 156–160.
35. Vijayakumar, A.; Du, T.; Sundaram, K. B. Characterization of Copper Indium Ditelluride/Electrolyte Interface Utilizing Electrochemical Impedance Spectroscopy. *Appl. Surf. Sci.* **2005**, *242*, 168–176.
36. Ananthan, M. R.; Kasiviswanathan, S. Growth and Characterization of Stepwise Flash Evaporated $CuInTe_2$ Thin Films. *Sol. Energy Mater. Sol. Cells* **2009**, *93*, 188–192.
37. Muftah, G. E. A.; Samantilleke, A. P. Electrochemical Deposition of $CuInTe_2$ Layers for Applications in Thin Film Solar Cells. *J. Mater. Sci.: Mater. Electron.* **2010**, *21*, 373–379.
38. Mise, T.; Nakada, T. Low Temperature Growth and Properties of Cu–In–Te Based Thin Films for Narrow Bandgap Solar Cells. *Thin Solid Films* **2010**, *518*, 5604–5609.
39. Bodnar, I. V.; Gurin, V. S.; Solovei, N. P.; Molochko, A. P. Formation and Optical Properties of $CuInTe_2$ Nanoparticles in Silicate Matrices. *Semiconductors* **2007**, *41*, 939–945.
40. Grisaru, H.; Palchik, O.; Gedanken, A. Microwave-Assisted Polyol Synthesis of $CuInTe_2$ and $CuInSe_2$ Nanoparticles. *Inorg. Chem.* **2003**, *42*, 7148–7155.
41. Neumann, H.; Mast, M.; Enderlein, J.; Tomlinson, R. D.; Yakushev, M. V. XPS Analysis of Bridgman-Grown $CuInTe_2$ and of Its Native Oxide. *Cryst. Res. Technol.* **1996**, *31*, 75–85.
42. Kucur, E.; Riegler, J.; Urban, G. A.; Nann, T. Determination of Quantum Confinement in CdSe Nanocrystals by Cyclic Voltammetry. *J. Chem. Phys.* **2003**, *119*, 2333–2337.
43. Lu, Q.; Hu, S.; Pang, D.; He, Z. Direct Electrochemistry and Electrocatalysis with Hemoglobin in Water-Soluble Quantum Dots Film on Glassy Carbon Electrode. *Chem. Commun.* **2005**, 2584–2585.
44. Querner, C.; Reiss, P.; Sadki, S.; Zagorska, M.; Pron, A. Size and Ligand Effects on the Electrochemical and Spectroelectrochemical Responses of CdSe Nanocrystals. *Phys. Chem. Chem. Phys.* **2005**, *7*, 3204–3209.
45. Poznyak, S. K.; Osipovich, N. P.; Shavel, A. S.; Talapin, D. V.; Gao, M.; Eychmüller, A.; Gaponik, N. Size-Dependent Electrochemical Behavior of Thiol-Capped CdTe Nanocrystals in Aqueous Solution. *J. Phys. Chem. B* **2005**, *109*, 1094–1100.
46. Inamdar, S. N.; Ingole, P. P.; Haram, S. K. Determination of Band Structure Parameters and the Quasi-Particle Gap of CdSe Quantum Dots by Cyclic Voltammetry. *ChemPhysChem* **2008**, *9*, 2574–2579.
47. Soreni-Harari, M.; Yaacobi-Gross, N.; Steiner, D.; Aharoni, A.; Banin, U.; Millo, O.; Tessler, N. Tuning Energetic Levels in Nanocrystal Quantum Dots through Surface Manipulations. *Nano Lett.* **2008**, *8*, 678–684.
48. Yue, W.; Han, S.; Peng, R.; Shen, W.; Geng, H.; Wu, F.; Tao, S.; Wang, M. $CuInS_2$ Quantum Dots Synthesized by a Solvothermal Route and Their Application as Effective Electron Acceptors for Hybrid Solar Cells. *J. Mater. Chem.* **2010**, *20*, 7570–7578.
49. Kim, S.; Im, S. H.; Kang, M.; Heo, J. H.; Seok, S. Il.; Kim, S.-W; Mora-Seró, I.; Bisquert, J. Air-Stable and Efficient Inorganic–Organic Heterojunction Solar Cells using PbS Colloidal Quantum Dots Co-Capped by 1-Dodecanethiol and Oleic acid. *Phys. Chem. Chem. Phys.*, **2012**, *14*, 14999–15002.

50. Chang, J. A.; Rhee, J. H.; Im, S. H.; Lee, Y. H.; Kim, H.-J.; Seok, S. I.; Nazeeruddin, M. K.; Grätzel, M. High-Performance Nanostructured Inorganic–Organic Heterojunction Solar Cells. *Nano Lett.* **2010**, *10*, 2609–2612.
51. Kim, S.; Kim, T.; Im, S. H.; Seok, S. I.; Kim, K. W.; Kim, S.; Kim, S.-W. Bandgap Engineered Monodisperse and Stable Mercury Telluride Quantum Dots and Their Application for Near-Infrared Photodetection. *J. Mater. Chem.* **2011**, *21*, 15232–15236.
52. Im, S. I.; Kim, H.-J.; Kim, S. W.; Kim, S.-W.; Seok, S. I. All Solid State Multiply Layered PbS Colloidal Quantum-Dot-Sensitized Photovoltaic Cells. *Energy Environ. Sci.* **2011**, *4*, 4181–4186.
53. Bodnar', I. V.; Gurin, V. S.; Soloveĭ, N. P.; Molochko, A. P. Formation and Optical Properties of $CuInTe_2$ Nanoparticles in Silicate Matrices. *Semiconductors* **2007**, *41*, 939–945.